Solid-State Electronics Vol. 33, No. 11, pp. 1425–1436, 1990
Printed in Great Britain

0038-1101/90 $3.00 + 0.00
Pergamon Press plc

THE EVOLUTION OF THE MINIMOS MOBILITY MODEL*

SIEGFRIED SELBERHERR,[1] WILFRIED HÄNSCH[2], MARDEN SEAVEY[3] and JAN SLOTBOOM[4]

[1]Technical University Vienna, Gußhausstraße 27-29/E360, A-1040 Wien, Austria, [2]Siemens Research Labs, Otto-Hahn-Ring 6, D-8000 München 83, F.R.G., [3]Digital Equipment Corp, 77 Reed Road, Hudson, MA 01749-2809, U.S.A. and [4]Philips Research Labs, P.O. Box 80000, N-5600 JA Eindhoven, The Netherlands

(Received 9 January 1990; in revised form 10 April 1990)

Abstract—The paper reviews the evolution of the mobility model of the MINIMOS program for the two-dimensional simulation of miniaturized MOS devices over a period of 10 years.

1. ABOUT CARRIER MOBILITIES

Carrier mobilities in semiconducting material are determined by a large variety of physical mechanisms. Electrons and holes are scattered by thermal lattice vibrations, ionized impurities, neutral impurities, vacancies, interstitials, dislocations, surfaces and electrons and holes themselves. A further mobility reduction is due to the saturation of the drift velocity of warm and hot carriers which is caused by lattice vibrations. Unfortunately, many of these mechanisms, especially their interactions, are extremely complicated and hence difficult to model. Principal reviews on that subject can be found in e.g. Refs[1,2].

The fundamental process for carrier scattering in a pure crystal is the interaction with the thermally generated vibrations of the atoms of the crystal. These lattice vibrations are a function of temperature. They yield a mobility component which we term $\mu_{n,p}^{L}$ (superscript L stands for lattice, subscripts n, p denote electrons or holes, respectively).

The next scattering mechanism to be considered is ionized impurity scattering. This effect causes a reduction of the pure lattice mobility. It is a function of the lattice temperature and the local concentration of ionized impurities. We term the mobility caused by lattice scattering and ionized impurity scattering $\mu_{n,p}^{LI}$.

In conjunction with ionized impurity scattering one should deal with neutral impurity scattering. However, since the impurities are almost completely ionized at temperatures above 77 K (liquid nitrogen) this effect is ignored. Another scattering mechanism which one should in principal take into account is carrier–carrier scattering. However, for miniaturized MOS devices it is of minor importance. It has always been neglected in the MINIMOS program.

The next scattering mechanism with which we have to deal is termed surface scattering. This effect is of obvious fundamental importance for MOS transistors. Theoretically, surface scattering is comprised of a good many different mechanisms like surface roughness scattering, scattering by interface charges and scattering by surface phonons. Although the application of MOS structures has received a great deal of attention in recent years, the problems associated with conduction at surfaces have not been investigated as deeply as one would expect. Therefore, all models which are presently used have been constructed on a fully empirical basis with a scope to reflect the main experimental findings as well as possible. Nevertheless, there exist obviously physical reasonings to support the empirical basis. We denote the account of surface scattering in a mobility expression with superscript S. We term the mobility caused by lattice scattering, ionized impurity scattering and surface scattering $\mu_{n,p}^{LIS}$.

The next phenomenon we consider is the saturation of the drift velocity for high electric field. This effect has to be accounted for by the reduction of the effective mobility since the magnitude of the drift velocity is the product of the mobility and the force which drives the carriers (to first order the electric field). $\mu_{n,p}^{LISF}$ denotes the mobility caused by lattice scattering, ionized impurity scattering, surface scattering and velocity saturation. It is the "effective" local mobility which we use for the two-dimensional analysis of the MOS device behavior.

The following sections describe the status of modeling the above described mechanisms for the carrier mobilities in terms of the evolution of the MINIMOS program.

2. THE MINIMOS 1 MOBILITY MODEL

The very first version of the MINIMOS program was completed in the summer of 1980[3]. The notation we use is different from that in the original paper in order to have a uniform appearance of all formulae.

*Dedicated to Professor Dr Hans Pötzl in honor of his 60th birthday.

2.1. Lattice scattering

The lattice mobility was modeled as temperature dependent with a simple power law.

$$\mu_n^L = 1430\,\mathrm{cm^2/V\,s}\cdot\left(\frac{T}{300\,\mathrm{K}}\right)^{-2,3},$$
$$\mu_p^L = 480\,\mathrm{cm^2/V\,s}\cdot\left(\frac{T}{300\,\mathrm{K}}\right)^{-2,2} \quad (1)$$

2.2. Ionized impurity scattering

Ionized impurity scattering was taken into account using the theoretical results of Refs[4] and[5]. CI is the total concentration of ionized impurities, i.e. the sum of ionized acceptors and donors $N_A^- + N_D^+$.

$$\mu_{n,p}^{LI} = \mu_{n,p}^L \cdot (1 + x^2 \cdot [Ci(x)\cdot\cos(x) + si(x)\cdot\sin(x)]) \quad (2)$$

with

$$x = \sqrt{\frac{6\cdot\mu_{n,p}^L}{\mu_{n,p}^I}} \quad (3)$$

$$\mu_n^I = \frac{1.4\times10^{14}\cdot\left(\frac{T}{300\,\mathrm{K}}\right)^{3/2}}{CI\cdot\mathcal{2}\left(\frac{1.69\times10^{10}\cdot\left(\frac{T}{300\,\mathrm{K}}\right)^2}{n}\right)},$$

$$\mu_p^I = \frac{1.08\times10^{14}\cdot\left(\frac{T}{300\,\mathrm{K}}\right)^{3/2}}{CI\cdot\mathcal{2}\left(\frac{2.78\times10^{10}\cdot\left(\frac{T}{300\,\mathrm{K}}\right)^2}{p}\right)} \quad (4)$$

$$\mathcal{2}(x) = \frac{1}{\ln(1+x) - \frac{x}{1+x}} \quad (5)$$

$$Ci(x) = -\int_x^\infty \frac{\cos(t)}{t}\cdot dt,$$
$$si(x) = -\int_x^\infty \frac{\sin(t)}{t}\cdot dt. \quad (6)$$

2.3. Surface scattering

The surface mobility was fitted with a dependence on the squareroot of the force pressing the carriers against the interface ($S_{n,p}$).

$$\mu_{n,p}^S = \mu_{n,p}^{ref}\cdot\sqrt{S_{n,p}^{ref}/S_{n,p}\cdot\frac{y+2\cdot y_{n,p}^{ref}}{2\cdot y_{n,p}^{ref}}}\Big/(S_{n,p}) \quad (7)$$

with:

$$\mu_n^{ref} = 447\,\mathrm{cm^2/V\,s}, \quad \mu_p^{ref} = 260\,\mathrm{cm^2/V\,s} \quad (8)$$
$$S_n^{ref} = 5\times10^3\,\mathrm{V/cm}, \quad S_p^{ref} = 2\times10^5\,\mathrm{V/cm} \quad (9)$$
$$y_n^{ref} = 10^{-7}\,\mathrm{cm}, \quad y_p^{ref} = 2\times10^{-7}\,\mathrm{cm} \quad (10)$$

y denotes the distance perpendicular to the interface. Note that eqn (7) is a fully phenomenological expression, neither the structure nor the associated parameters may be claimed to be correct in a theoretical sense.

The interface pressing forces $S_{n,p}$ were modeled with eqn (11). They are simply the electric field perpendicular to current flow.

$$S_{n,p} = \frac{\max(0, \vec{E}\times\vec{J}_{n,p})}{|\vec{J}_{n,p}|}. \quad (11)$$

2.4. Velocity saturation

The structure of the formula used for the "effective" mobility is a three term weighted Mathiessen rule:

$$\mu_{n,p}^{LISF} = \mu_{n,p}^{LI}\Big/\left\{\left(1+\left(\mu_{n,p}^{LI}\cdot\sqrt{\left(\frac{1}{\mu_{n,p}^S}\right)^2+\left(\frac{F_{n,p}}{v_{n,p}^{sat}}\right)^2}\right)^{\beta_{n,p}}\right)^{1/\beta_{n,p}}\right\} \quad (12)$$

with

$$\beta_n = 1.11\cdot\left(\frac{T}{300\,\mathrm{K}}\right)^{0.66}, \quad \beta_p = 1.21\cdot\left(\frac{T}{300\,\mathrm{K}}\right)^{0.17}. \quad (13)$$

The temperature dependence of the coefficients eqn (13) is from Ref.[6].

F_n and F_p, the effective driving forces, were given by eqn (14). They are simply the electric field parallel to current flow.

$$F_{n,p} = \frac{\max(0, \vec{E}\cdot\vec{J}_{n,p})}{|\vec{J}_{n,p}|} \quad (14)$$

The carrier saturation velocities $v_{n,p}^{sat}$ were modeled as temperature dependent with formulae (15) interpreting the results of Ref.[6]. Additionally, a reduction of the saturation velocity directly at the surface by a factor of two was modeled. Those days it was the general belief that the saturation velocity in an inversion layer is smaller than the bulk value. The characteristic distance y^{ref} is the same used for surface scattering; it is given with eqn (10).

$$v_n^{sat} = 10^7\,\mathrm{cm/s}\cdot\left(\frac{T}{300\,\mathrm{K}}\right)^{-0.87}\cdot\frac{y+y_n^{ref}}{y+2\cdot y_n^{ref}},$$
$$v_p^{sat} = 8.34\times10^6\,\mathrm{cm/s}\cdot\left(\frac{T}{300\,\mathrm{K}}\right)^{-0.52}\cdot\frac{y+y_p^{ref}}{y+2\cdot y_p^{ref}} \quad (15)$$

3. THE MINIMOS 2 MOBILITY MODEL

A major new version of MINIMOS was announced in 1982[7,8].

3.1. Lattice scattering

The model for the lattice mobility was kept from MINIMOS 1 with eqn (1).

3.2. Ionized impurity scattering

For ionized impurity scattering the heuristic and significantly simpler expression given by Caughey

and Thomas[9] was taken with a minimum of temperature dependent coefficients, since the more complex theoretically founded model eqn (2) did not deliver sufficiently satisfying results.

$$\mu_{n,p}^{\mathrm{LI}} = \mu_{n,p}^{\min} + \frac{\mu_{n,p}^{\mathrm{L}} - \mu_{n,p}^{\min}}{1 + (CI/C_{n,p}^{\mathrm{ref}})^{\alpha_{n,p}}} \tag{16}$$

with:

$$\mu_n^{\min} = 55.24\ \mathrm{cm^2/V\,s},$$
$$\mu_p^{\min} = 49.7\ \mathrm{cm^2/V\,s} \tag{17}$$
$$C_n^{\mathrm{ref}} = 1.072 \times 10^{17}\ \mathrm{cm^{-3}} \cdot \left(\frac{T}{300\ \mathrm{K}}\right)^{2.97},$$
$$C_n^{\mathrm{ref}} = 1.606 \times 10^{17}\ \mathrm{cm^{-3}} \cdot \left(\frac{T}{300\ \mathrm{K}}\right)^{3.1} \tag{18}$$
$$\alpha_n = 0.7, \quad \alpha_p = 0.73 \tag{19}$$

3.3. Surface scattering

Regarding surface scattering and velocity saturation Thornber[10] has made a suggestion, which is well accepted today, to use a relation of the form eqn (20) for the total effective mobility.

$$\mu_{n,p}^{\mathrm{LISF}} = \mu_{n,p}^{\mathrm{LISF}}(\mu_{n,p}^{\mathrm{LIS}}(\mu_{n,p}^{\mathrm{LI}}, S_{n,p}), F_{n,p}, v_{n,p}^{\mathrm{sat}}) \tag{20}$$

With this knowledge the following expression for the influence of surface scattering was developed[11,12].

$$\mu_{n,p}^{\mathrm{LIS}} = \mu_{n,p}^{\mathrm{LI}} \cdot \frac{y + y_{n,p}^{\mathrm{ref}}}{y + b_{n,p} \cdot y_{n,p}^{\mathrm{ref}}} \tag{21}$$

with:

$$y_n^{\mathrm{ref}} = (5 \times 10^{-7}\ \mathrm{cm}) \Big/ \left(1 + \frac{F_n}{10^4\ \mathrm{V/cm}}\right),$$
$$y_p^{\mathrm{ref}} = (4 \times 10^{-7}\ \mathrm{cm}) \Big/ \left(1 + \frac{F_p}{8 \times 10^3\ \mathrm{V/cm}}\right) \tag{22}$$
$$b_n = 2 + \frac{S_n}{1.8 \times 10^5\ \mathrm{V/cm}},$$
$$b_p = 2 + \frac{S_p}{3.8 \times 10^5\ \mathrm{V/cm}}. \tag{23}$$

Directly at the interface the mobility is reduced by a factor $1/b$; at a distance $y = y^{\mathrm{ref}}$ it is reduced by the factor $2/(1+b)$; and at greater distance from the surface it naturally follows that the reduction factor approaches unity. y^{ref} represents a characteristic length which describes the range of influence of the surface.

This range is modeled as a function of the carrier driving force $F_{n,p}$. The formulation of y^{ref} produces a reduction in the range of influence of surface scattering for greater driving forces, and thereby velocity saturation appears. Carriers already traveling with the saturation velocity can be considered not to experience the influence of the surface as much as cold carriers[13]. The parameter b in eqn (21) describes the strength of the influence of surface scattering and is modeled as a function of $S_{n,p}$. The formulation of b rests upon the consideration that the charge carriers are presented against the surface by an electric field, which results in a greater scattering, in such a way that a greater mobility reduction occurs. Without any electric field we also observe a mobility reduction due to surface roughness scattering ($b = 2$). Equation (21) is again a fully phenomenological expression which is not claimed to be correct in a theoretical sense. It simply represented experience which had been confirmed over several years by many users of our simulation tools that an expression with such a structure nicely reflects experimental observations.

For the interface pressing forces, the respective equations of MINIMOS 1, eqn (11), have been kept.

3.4. Velocity saturation

Velocity saturation is then accounted with eqn (24) which is a weighted Mathiessen rule.

$$\mu_{n,p}^{\mathrm{LISF}} = \mu_{n,p}^{\mathrm{LIS}} \Big/ \left(1 + \left(\frac{\mu_{n,p}^{\mathrm{LIS}} \cdot F_{n,p}}{v_{n,p}^{\mathrm{sat}}}\right)^{\beta_{n,p}}\right)^{1/\beta_{n,p}} \tag{24}$$

with:

$$\beta_n = 2, \quad \beta_p = 1 \tag{25}$$

The temperature dependence of the Mathiessen coefficients eqn (25) has been dropped. The same carrier driving forces were used as in MINIMOS 1, cf. eqn (14).

The carrier saturation velocities were modeled as temperature dependent only with formulae (26) using the results of Ref.[6]. Any reduction of the saturation velocities in the inversion layer has been dropped.

$$v_n^{\mathrm{sat}} = 10^7\ \mathrm{cm/s} \cdot \left(\frac{T}{300\ \mathrm{K}}\right)^{-0.87},$$
$$v_p^{\mathrm{sat}} = 8.34 \times 10^6\ \mathrm{cm/s} \cdot \left(\frac{T}{300\ \mathrm{K}}\right)^{-0.52}. \tag{26}$$

4. THE MINIMOS 3 MOBILITY MODEL

A major new version of MINIMOS was announced in 1986[14].

4.1. Lattice scattering

The coefficients of the lattice mobility have been adjusted in order to decrease the mobility slightly eqn (27). The motivation to do so came from Ref.[15] which was generally accepted at that time.

$$\mu_n^{\mathrm{L}} = 1252\ \mathrm{cm^2/V\,s} \cdot \left(\frac{T}{300\ \mathrm{K}}\right)^{-2.33},$$
$$\mu_p^{\mathrm{L}} = 407\ \mathrm{cm^2/V\,s} \cdot \left(\frac{T}{300\ \mathrm{K}}\right)^{-2.23}. \tag{27}$$

4.2. Ionized impurity scattering

Also by following the work in Ref.[15] the influence of ionized impurity scattering was treated. The formula is structurally similar to the formula (16)

used in MINIMOS 2.

$$\mu_{n,p}^{\mathrm{LI}} = \mu_{n,p}^{\min} + \frac{\mu_{n,p}^{\mathrm{L}}}{1 + (CI/C_{n,p}^{\mathrm{ref}})^{\alpha_{n,p}}} \tag{28}$$

with:

$$\mu_n^{\min} = 88\ \mathrm{cm^2/V\,s} \cdot \left(\frac{T}{300\ \mathrm{K}}\right)^{-0.57},$$

$$\mu_p^{\min} = 54.3\ \mathrm{cm^2/V\,s} \cdot \left(\frac{T}{300\ \mathrm{K}}\right)^{-0.57} \tag{29}$$

$$C_n^{\mathrm{ref}} = 1.26 \times 10^{17}\ \mathrm{cm^{-3}} \cdot \left(\frac{T}{300\ \mathrm{K}}\right)^{2.4},$$

$$C_p^{\mathrm{ref}} = 5.875 \times 10^{-6}\ \mathrm{cm^{-3}} \cdot \left(\frac{T}{300\ \mathrm{K}}\right)^{2.4}. \tag{30}$$

$$\alpha_{n,p} = 0.88 \cdot \left(\frac{T}{300\ \mathrm{K}}\right)^{-0.146}. \tag{31}$$

4.3. *Surface scattering*

Surface scattering was modeled with the theoretically founded formula, eqn (32).

$$\mu_{n,p}^{\mathrm{LIS}} = \mu_{n,p}^{\mathrm{LI}} \Bigg/ \left[1 + \frac{\mathscr{G}_{n,p}(y)}{1 + \mathscr{G}_{n,p}(y)^2} \cdot \left(\frac{\mu_{n,p}^{\mathrm{LI}} \cdot S_{n,p}}{v_{n,p}^{\mathrm{sat}}}\right)^2\right] \tag{32}$$

with:

$$\mathscr{G}_{n,p}(y) = g_{n,p} \cdot \exp\left(\left(\frac{y}{y_{n,p}^{\mathrm{ref}}}\right)^2\right) \tag{33}$$

$$g_n = 0.09, \quad g_p = 0.1 \tag{34}$$

$$y_n^{\mathrm{ref}} = 1.9 \times 10^{-8}\ \mathrm{cm}, \quad y_p^{\mathrm{ref}} = 3.1 \times 10^{-8}\ \mathrm{cm} \tag{35}$$

To derive eqn (32) from the fundamental hydrodynamic equations an anisotropic momentum relaxation time tensor $(\tau_{\mathrm{m}}^{-1})_{n,p}$ was introduced, eqn (36):

$$(\tau_{\mathrm{m}}^{-1})_{n,p} = \begin{pmatrix} (\tau_{\mathrm{m,bulk}}^{-1})_{n,p} & 0 & 0 \\ 0 & (\tau_{\mathrm{m,bulk}}^{-1})_{n,p} + (\tau_{\mathrm{m,surf}}^{-1})_{n,p} & 0 \\ 0 & 0 & (\tau_{\mathrm{m,bulk}}^{-1})_{n,p} \end{pmatrix} \tag{36}$$

Here the yy element refers to the component perpendicular to the surface and the xx and zz elements to those parallel to the interface. The surface momentum relaxation time $\tau_{\mathrm{m,surf}}$ prevents the current from penetrating through the surface. For the limit $\tau_{\mathrm{m,bulk}} \gg \tau_{\mathrm{m,surf}}$ we obtain for the mobility at the interface $y = 0$:

$$\mu_{n,p}^{\mathrm{LIS}} = \frac{\mu_{n,p}^{\mathrm{LI}}}{1 + \mathscr{R}_{np} \cdot (S_{n,p})^2} \tag{37}$$

with:

$$\mathscr{R}_{n,p} = \frac{(\tau_{\mathrm{m,surf}})_{n,p}}{(\tau_{\mathrm{m,bulk}})_{n,p}} \cdot \left(\frac{\mu_{n,p}^{\mathrm{LI}}}{v_{n,p}^{\mathrm{sat}}}\right)^2. \tag{38}$$

Equation (38) was then modeled introducing a dependence on the distance to the interface y and we ended up with eqns (32) and (33).

Although we have found with the assumption eqn (36) the correct qualitative behavior of the gate field reduced channel mobility eqn (37), its usefulness for quantitative modeling was poor. The reason for this lies in the fact that the anisotropic momentum relaxation time, eqn (36), is too simple an approximation to account for surface scattering. Furthermore, the interpolation into the bulk with eqn (33) is somewhat arbitrary because the scale on which this function varies is not *a priori* known. Our first attempt was to introduce a scale $y_{n,p}^{\mathrm{ref}}$ of the order of a few Angstroms which is the range of the surface states into the bulk. This led to a rapid variation of the surface mobility over the extension of the inversion channel which caused the terminal currents to be very sensitive to $y_{n,p}^{\mathrm{ref}}$. Later we developed a surface mobility that was based on the solution of the Boltzmann equation in the vicinity of the interface[16]. This investigation showed that the influence of surface scattering cannot be simply represented by eqn (36). The surface properties enter through a scattering parameter p that ranges from 0 to 1 and covers total diffusive to completely reflective surfaces. We found that the explicit spatial variation is of the order 5–10 nm depending on the scattering parameter p. A larger value of p leads to a larger $y_{n,p}^{\mathrm{ref}}$. The scattering parameter p enters the boundary condition for the distribution function and has only a very indirect link to a macroscopic momentum relaxation time $(\tau_{\mathrm{m,surf}})_{n,p}$ as proposed in eqn (36). Indeed it is shown that surface scattering will effect both components of the tensor eqn (36). Although the exact result is very complicated, it is possible to extract a simple analytical fit formula which is very similar to the surface mobility introduced in MINIMOS 4 [cf. eqn (51)].

$$\mu_{n,p}^{\mathrm{LIS}} = \frac{\mu_{n,p}^{\mathrm{LI}} + (\mu_{n,p}^{\mathrm{ref}} - \mu_{n,p}^{\mathrm{LI}}) \cdot \mathscr{F}(y)}{1 + \mathscr{F}(y) \cdot \frac{1}{2} \cdot (1-p)(S_{n,p}/S_{n,p}^{\mathrm{ref}})^{1/2 \cdot (1+p)}} \tag{39}$$

with:

$$\mathscr{F}(y) = \exp\left(-\left(\frac{y}{10 \cdot \lambda_{\mathrm{th}}}\right)^2\right). \tag{40}$$

Here λ_{th} is the thermal wave length and $S_{n,p}^{\mathrm{ref}} = U_{\mathrm{th}}/\lambda_{\mathrm{th}}$, with the thermal voltage U_{th}. In Fig. 1 we compare the exact result with the fit formula eqn (39) for zero field and a scattering parameter $p = 0.5$. This figure clearly shows the intrinsic spatial dependence of the channel mobility indeed is constant within 5 nm from the surface. In Fig. 2 we show the variation of the exact result and the fit formula eqn (39) for an exponentially decreasing interface pressing force with

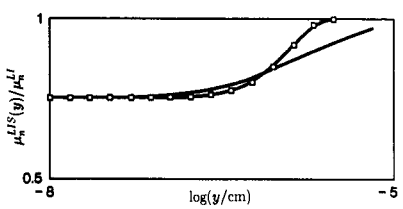

Fig. 1. $\mu_n^{\mathrm{LIS}}(y)/\mu_n^{\mathrm{LI}}$ for zero pressing force; exact result, ——; fit formula (39) □; $p = 0.5$.

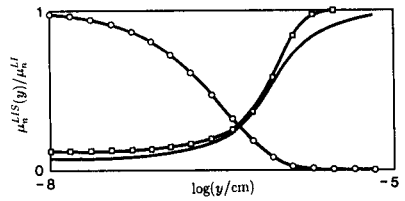

Fig. 2. $\mu_n^{LIS}(y)/\mu_n^{LI}$ for exponentially decreasing pressing force with maximum $S_n = 6 \times 10^5$ V/cm; exact result ——; fit formula (39) □; $p = 0.5$.

the maximum value $S = 5 \times 10^5$ V/cm at the surface. Although we find a considerable decrease of the surface field the mobility shows only a weak variation near the surface as long $y < 5$ nm. In Fig. 3 we show the field dependence of the ratio μ_n^{ref}/μ_n^{LI} at the interface $y = 0$. Again we compare the exact result with eqn (39) for two different scattering parameters $p = 0.5$ and $p = 0.9$. There is a very good agreement for the larger value of p. From fitting the exact results to a real I–V characteristic of a device[16] it was found that for n- and p-channel MOSFETs a scattering parameter $p > 0.8$ is required. This means that the SiO_2/Si interface is almost perfect. From this we can conclude that a surface mobility of the form eqn (39) will be very suitable for modeling.

The interface pressing forces $S_{n,p}$ in eqns (32) and (39) are modeled with eqn (41).

$$S_n = \max\left(0, \frac{\partial \psi}{\partial y}\right), \quad S_p = \max\left(0, -\frac{\partial \psi}{\partial y}\right). \tag{41}$$

4.4. Velocity saturation

Velocity saturation is modeled with formulae (42). These are again fits to experimental data with, however, a theoretical background used in their functional form[17–19].

$$\mu_n^{LISF} = (2 \cdot \mu_n^{LIS}) \Big/ 1 + \sqrt{1 + \left(\frac{2 \cdot \mu_n^{LIS} \cdot F_n}{v_n^{sat}}\right)^2},$$

$$\mu_p^{LISF} = (\mu_p^{LIS}) \Big/ \left(1 + \frac{\mu_p^{LIS} \cdot F_p}{v_p^{sat}}\right) \tag{42}$$

F_n and F_p, the effective driving forces, are given by eqn (43). Their derivation can be found in Ref.[14].

$$F_n = \left| \text{grad}\, \psi - \frac{1}{n} \cdot \text{grad}(Ut_n \cdot n) \right|,$$

$$F_p = \left| \text{grad}\, \psi + \frac{1}{p} \cdot \text{grad}(Ut_p \cdot p) \right| \tag{43}$$

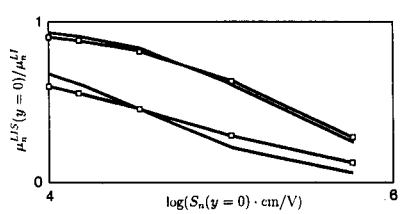

Fig. 3. $\mu_n^{LIS}(y)/\mu_n^{LI}$ for $y = 0$; $p = 0.9$ upper curves; $p = 0.5$ lower curves; exact result ——; fit formula (39) □.

Driving force $F_{n,p}$, mobility $\mu_{n,p}^{LISF}$, and carrier voltage $Ut_{n,p}$ are coupled to each other as shown in Ref. [14]. Therefore it can lead to erroneous conclusions if one of these quantities is considered independently from the others.

The saturation velocities were still modeled with simple power laws, eqn (44), but the value for electrons has been raised by 7%.

$$v_n^{sat} = 1.07 \times 10^7 \text{ cm/s} \cdot \left(\frac{T}{300 \text{ K}}\right)^{-0.87},$$

$$v_p^{sat} = 8.34 \times 10^6 \text{ cm/s} \cdot \left(\frac{T}{300 \text{ K}}\right)^{-0.52}. \tag{44}$$

4.5. Anisotropic mobility

Tests have been made with an anisotropic mobility using eqn (45). However, this attempt was not really successful.

$$\mu_{n,p}^{*} = \mu_{n,p}^{LISF} \cdot \begin{pmatrix} 1 & 0 & 0 \\ 0 & 1 - \dfrac{1}{1 + \mathscr{G}(y) \cdot (\mu_{n,p}^{LI}/\mu_{n,p}^{LISF})} & 0 \\ 0 & 0 & 1 \end{pmatrix} \tag{45}$$

The anisotropic mobility was based on eqn (36). This assumption was too simple as discussed above. However, the idea of an anisotropy mobility cannot be disregarded for physical reasons. The interface has a symmetry breaking effect in the device and therefore the directions parallel and perpendicular to the interface should be distinguished. This anisotropy will, however, not be important for the inversion channel because there the dominant charge transport is parallel to the interface and the perpendicular component can be neglected. In the saturation region we have velocity saturation and with good approximation we can disregard surface effects on the saturation velocity. Therefore we believe that for practical considerations an isotropic mobility is sufficient as long as it correctly describes the situation in the inversion channel.

5. THE MINIMOS 4 MOBILITY MODEL

The best established version of MINIMOS has been made publicly available in 1988[20].

5.1. Lattice scattering

The lattice mobility is still fitted with simple power laws. The mobility has been increased compared to MINIMOS 3. These expressions fit well experimental data of Refs [6,17,21].

$$\mu_n^L = 1430 \text{ cm}^2/\text{V s} \cdot \left(\frac{T}{300 \text{ K}}\right)^{-2},$$

$$\mu_p^L = 460 \text{ cm}^2/\text{V s} \cdot \left(\frac{T}{300 \text{ K}}\right)^{-2.18} \tag{46}$$

5.2. Ionized impurity scattering

For ionized impurity scattering the functional form eqn (16) of the fit provided by Caughey and Thomas[12] is taken (as it was in MINIMOS 2) and improved temperature dependent coefficients are used.

$$\mu_n^{\min} = \begin{cases} 80\ \mathrm{cm^2/V\,s} \cdot \left(\dfrac{T}{300\ \mathrm{K}}\right)^{-0.45} & T \geqslant 200\ \mathrm{K} \\ 80\ \mathrm{cm^2/V\,s} \left(\dfrac{200\ \mathrm{K}}{300\ \mathrm{K}}\right)^{-0.45} \cdot \left(\dfrac{T}{200\ \mathrm{K}}\right)^{-0.15} & T < 200\ \mathrm{K} \end{cases} \tag{47}$$

with:

$$\mu_p^{\min} = \begin{cases} 45\ \mathrm{cm^2/V\,s} \cdot \left(\dfrac{T}{300\ \mathrm{K}}\right)^{-0.45} & T \geqslant 200\ \mathrm{K} \\ 45\ \mathrm{cm^2/V\,s} \left(\dfrac{200\ \mathrm{K}}{300\ \mathrm{K}}\right)^{-0.45} \cdot \left(\dfrac{T}{200\ \mathrm{K}}\right)^{-0.15} & T < 200\ \mathrm{K} \end{cases} \tag{48}$$

$$C_n^{\mathrm{ref}} = 1.21 \times 10^{17}\ \mathrm{cm^{-3}} \cdot \left(\frac{T}{300\ \mathrm{K}}\right)^{3.2},$$

$$C_p^{\mathrm{ref}} = 2.23 \times 10^{17}\ \mathrm{cm^{-3}} \cdot \left(\frac{T}{300\ \mathrm{K}}\right)^{3.2} \tag{49}$$

$$\alpha^{n,p} = 0.72 \cdot \left(\frac{T}{300\ \mathrm{K}}\right)^{0.065} \tag{50}$$

The fits eqns (47)–(50) are from Ref.[22]. Similar data have been provided in Ref.[23].

5.3. Surface scattering

Surface scattering is modeled with the following expressions.

$$\mu_{n,p}^{\mathrm{LIS}} = \frac{\mu_{n,p}^{\mathrm{ref}} + (\mu_{n,p}^{\mathrm{LI}} - \mu_{n,p}^{\mathrm{ref}}) \cdot [1 - \mathscr{F}(y)]}{1 + \mathscr{F}(y) \cdot (S_{n,p}/S_{n,p}^{\mathrm{ref}})^{\gamma n,p}} \tag{51}$$

with:

$$\mu_n^{\mathrm{ref}} = \frac{638\ \mathrm{cm^2/V\,s}}{MR} \cdot \left(\frac{T}{300\ \mathrm{K}}\right)^{-1.19},$$

$$\mu_p^{\mathrm{ref}} = \frac{106\ \mathrm{cm^2/V\,s}}{MR} \cdot \left(\frac{T}{300\ \mathrm{K}}\right)^{-1.09} \tag{52}$$

$$\mathscr{F}(y) = \frac{2 \cdot \exp(-(y/10\ \mathrm{nm})^2)}{1 + \exp(-2 \cdot (y/10\ \mathrm{nm})^2)} \tag{53}$$

$$S_n^{\mathrm{ref}} = \frac{7 \times 10^5\ \mathrm{V/cm}}{MT}, \quad S_p^{\mathrm{ref}} = \frac{2.7 \times 10^5\ \mathrm{V/cm}}{MT} \tag{54}$$

$$\gamma_n = \frac{1.3}{MX}, \quad \gamma_p = \frac{1}{MX}. \tag{55}$$

In the above expressions, MR, MT and MX are fit parameters which generally are close to unity. Particularly when utilizing also the improved fits eqns (67) and (68) the mobility parameters have been shown to be valid (i.e. $MR = MT = MX = 1$) at 300 K ambient temperature over wide ranges of electric fields, oxide thicknesses and doping concentrations, using data from a number of independent sources (see also Ref.[24]). Limited verification has been done as a function of temperature, nevertheless, the fits in eqn (52) appear to be approximately correct.

The interface pressing forces are again modeled with eqn (41).

Note from eqn (53) that for $y = 0$, i.e. at the oxide–silicon interface, $\mathscr{F}(y) = \mathscr{F}(0) = 1$. Thus from eqn (51) we obtain:

$$\mu_{n,p}^{\mathrm{LIS}} = \frac{\mu_{n,p}^{\mathrm{ref}}}{1 + (S_{n,p}/S_{n,p}^{\mathrm{ref}})^{\gamma n,p}} \tag{56}$$

This has the form of the "universal" mobility equation[25,26], except of course $\mu_{n,p}^{\mathrm{LIS}}$ is a local quantity.

The function $\mathscr{F}(y)$ is an arbitrary chosen function which provides a continuous transition from surface to bulk. It has the property of remaining relatively flat over the extent of the inversion layer; e.g. $\mathscr{F}(y)$ decreases by only 3% over the first 5 nm below the interface.

To connect the local mobility eqn (51) with measureable quantities, it is necessary to define an effective mobility and an effective field as follows:

$$\mu^{\mathrm{eff}} = \frac{\int_0^\infty \mu_n^{\mathrm{LIS}} \cdot n \cdot \mathrm{d}y}{\int_0^\infty n \cdot \mathrm{d}y} \tag{57}$$

$$E^{\mathrm{eff}} = \frac{\int_0^\infty S \cdot n \cdot \mathrm{d}y}{\int_0^\infty n \cdot \mathrm{d}y} \tag{58}$$

These two equations are easily implemented in MINIMOS. μ^{eff} and E^{eff} have to be evaluated in MINIMOS at the center of the channel between the source and drain for relatively long channel devices. Then the connection between μ^{eff} and E^{eff}, as computed by MINIMOS, and measurable quantities is as follows:

$$\mu^{\mathrm{eff}} = \frac{I_{\mathrm{DS}} \cdot L^{\mathrm{eff}}}{W^{\mathrm{eff}} \cdot Q^{\mathrm{inv}} \cdot V_{\mathrm{DS}}} \tag{59}$$

$$E^{\mathrm{eff}} = (Q^{\mathrm{bulk}} + \tfrac{1}{2} \cdot Q^{\mathrm{inv}})/\epsilon_{\mathrm{Si}} \tag{60}$$

with:

$$Q^{\mathrm{bulk}} = \eta \cdot C_{\mathrm{ox}} \cdot \sqrt{2 \cdot \varphi_{\mathrm{f}} - V_{\mathrm{BS}}} \tag{61}$$

$$Q^{\mathrm{inv}} = q \cdot \int_0^\infty n \cdot \mathrm{d}y = C_{\mathrm{ox}} \cdot (V_{\mathrm{GS}} - V_{\mathrm{threshold}}) \tag{62}$$

In the above equations I_{DS} is the drain current, L^{eff} and W^{eff} are the effective channel length and effective channel width, respectively, V_{DS} is the applied drain to source voltage, Q^{bulk} and Q^{inv} are the bulk charge per cm^2 and the free carrier charge per cm^2, respectively, ϵ_{Si} is the silicon dielectric constant, C_{ox} is the gate oxide capacitance, V_{GS} is the gate to source voltage, $V_{threshold}$ is the extrapolated threshold voltage, V_{BS} is the bulk to source voltage, and η and φ_f are the substrate sensitivity factor and Fermi potential at strong inversion, respectively.

For improved accuracy, Q^{bulk} and Q^{inv} may be obtained by the AC split C–V method[27]. However, the formula eqn (59) is not strictly valid in subthreshold[28,29] (in particular, see eqns (1) and (2) of Ref. [7]. Because of the dominance of diffusion in the subthreshold, knowledge of the inversion charge density is insufficient for a determination of the drain current.

An application of eqn (59), together with an accurate determination of Q^{inv}, can lead to an erroneous roll-off of effective mobility with effective field. This is shown in Fig. 4. The upper curve is the true effective mobility as computed from eqn (57), and the lower curve is the "measured" mobility obtained using eqn (59). The total Q^{inv} in the inversion layer, referred to in Fig. 4, is the average inversion charge per unit area obtained by integrating the local Q^{inv} from the effective source edge to the effective drain edge, and thus this total Q^{inv} should closely approximate what would be obtained experimentally by the split C–V method. The pronounced roll-off of the "measured" mobility is evident in the lower curve. This spurious mobility roll-off may account for the apparent mobility roll-off at low gate voltages reported in Ref. [30].

The local mobility quantities appearing in eqns (52), (54) and (55) cannot be directly extracted. However, these quantities do not differ too greatly from the corresponding ones in the "universal" mobility formula which connects μ^{eff} and E^{eff}:

$$\mu^{eff} = \frac{\mu^{surf}}{1 + (E^{eff}/E^{ref})^{\gamma^{eff}}} \tag{63}$$

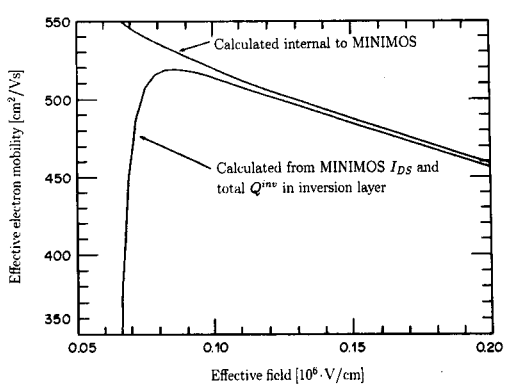

Fig. 4. Comparison of effective mobilities from MINIMOS 4.

At low enough pressing forces, eqn (63) corresponds closely to eqn (56) because $S_{n,p}$ in eqn (56) then varies only slightly over the inversion layer. The parameters μ^{surf}, E^{ref} and γ^{eff} extracted from the "universal" curve are good starting values for finding by trial and error the corresponding values in the local mobility formula (51). This was the method originally used by one of us (the DIGITAL author) to extract the mobility parameters $\mu_{n,p}^{ref}$, $S_{n,p}^{ref}$ and $\gamma_{n,p}$ from measurements. The values extracted at that time (October 1986) do not differ greatly from the values listed in eqn (52) with eqn (67), eqns (54) and (55) with eqn (68) which are based on a significantly wider range of data.

The formulae discussed here for surface scattering are still not the ultimate expressions. They just fit quite reasonably experimental observations. Other approaches with the same claim can be found in, e.g. Refs [31,32]. A u-shaped mobility behavior as found in Ref. [33] for application at liquid nitrogen ambient temperature has not been synthesized because we do not believe in surface scattering as origin for this experimental observation.

5.4. *Velocity saturation*

The model for velocity saturation is the same as in MINIMOS 3, cf. eqn (42). Also the models for the effective driving forces eqn (43) have proven to be adequate.

The saturation velocities are presently modeled with formulae (64).

$$v_n^{sat} = 1.45 \times 10^7 \text{ cm/s} \cdot \sqrt{\tanh\left(\frac{155 \text{ K}}{T}\right)},$$

$$v_n^{sat} = 9.05 \times 10^6 \text{ cm/s} \cdot \sqrt{\tanh\left(\frac{312 \text{ K}}{T}\right)} \tag{64}$$

The functional form of these fits is after Ref. [17]; the experimental data matched are from Refs [5,6,17,34,35]. An eventual dependence on the crystallographic orientation which one would deduce from[36–38] is presently not taken into account.

6. EVALUATION OF THE MINIMOS 4 MOBILITY MODEL

6.1. *The perspective of a DIGITAL researcher*

The MINIMOS 4 program is the basic two-dimensional device simulation program at use in DIGITAL. Coupled with process simulation programs, MINIMOS 4 serves as the principal design aid for new CMOS transistor structures. In addition, MINIMOS 4 is of aid in circuit design as a predictor of worst case conditions for a given CMOS process. The procedure is to fine tune the mobility parameters to closely match average measured I–V data over a wide range of bias conditions. Then I–V data are generated at extremes of channel length, oxide thickness, doping profile variations, etc. to establish worst case conditions. The MINIMOS 4 mobility model has proven very useful in this worst case file design.

The mobility model eqn (51) due to surface scattering has been employed at DIGITAL since October 1986 with good success. The fit parameters *MR*, *MT* and *MX* defined in eqns (52), (54) and (55) are generally close to unity. However, for certain experimental processes one or more of these parameters may deviate significantly from unity. When such deviations occur, they are usually accompanied by other effects such as anomalous threshold voltage dependencies and/or changed subthreshold leakage. The extent to which the mobility model needs to be adjusted becomes a good indicator of possible peculiarities in the process, such as unusual surface state generation, or polysilicon doping irregularities. As dimensions shrink toward the sub-half micron region, such peculiarities will clearly become more critical, and the mobility modeling will require increased scrutiny.

6.2. The perspective of a Philips researcher

Modeling of the carrier mobility in the inversion layer of MOSFET transistors is of crucial importance for accurate device characterization. Several authors[23,30,39,40] have shown that the normal electric field dependence of the mobility is described by a "universal" curve if the measurements are analyzed in terms of an effective normal electric field. It appeared that the substrate impurity concentration and the back-bias voltage are of little influence on this curve and it can be considered as a reproducible property of the Si/SiO_2 interface.

The effective normal electric field is the averaged pressing force over the electron distribution in the inversion layer eqn (58).

Because the mobilities are measured as a function of this effective electric field, it seems straightforward to implement these data by means of a "global" mobility model[41] into a device simulator and assuming that the electrons in the inversion layer feel the same effective electric field. However, such a non-local approach introduces numerical problems because in other regions of the device local quantities are used. It is also numerically inefficient compared to local models. The question arises: If we use the local MINIMOS 4 mobility model, how well does it agree with the empirical "universal" mobility curve if the calculations are interpreted, just as the measurements, in terms of an effective electric field? In particular, we investigated[24] the surface scattering mobility model (51) embedded in the total MINIMOS 4 mobility model.

In a post-processor the calculated local quantities are analyzed in terms of the effective normal electric field and effective mobility. In this way we simulate the experimental procedure. The total channel current is given by:

$$I_{DS} = q \cdot \mu^{eff} \cdot Q^{inv} \cdot \frac{d\varphi_n}{dx} \tag{65}$$

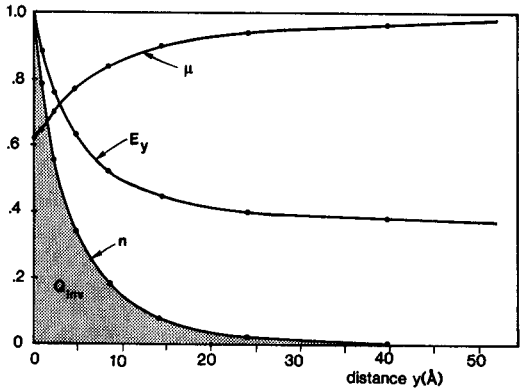

Fig. 5. Calculated electron concentration, normal electric field and mobility in the inversion layer; the norm factors are $5.8 \times 10^{19}\,cm^{-3}$, 7.2×10^5 V/cm and $506\,cm^2/(V\,s)$. ($t_{ox} = 17.5$ nm, $N_{sub} = 1.8 \times 10^{17}\,cm^{-3}$, $V_{GS} = 5$ V, $V_{DS} = 0.1$ V.)

where Q^{inv} is the inversion layer charge density eqn (62) and φ_n is the electron quasi-Fermi potential. The effective mobility is easily derived from eqn (65) because I_{DS}, Q^{inv} and $d\varphi_n/dx$ are known. The calculations are done for $V_{DS} = 0.1$ V. Assuming that in the inversion channel $\varphi_n(y) = \text{const.}$ eqn (58) can be integrated and gives:

$$E^{eff} = \frac{k_B \cdot T}{q} \cdot n(0)/Q^{inv} \tag{66}$$

where $n(0)$ is the electron concentration at the interface. Figure 5 is an example of the calculations where both the variation of the local quantities over the channel as well as the effective mobility and effective electric field are shown.

A number of transistors, varying in substrate doping concentration between $4 \times 10^{15}\,cm^{-3}$ to $2 \times 10^{18}\,cm^{-3}$ and in gate oxide thickness between 30 and 10 nm have been simulated with MINIMOS 4. As described above, we have extracted the effective mobility curves for *n*-channel and *p*-channel transistors up to very high electric fields, and compared with experimental data[25,30,39,40].

The thereby optimized mobility parameters eqns (67) and (68) give corrections to the default values eqns (52) and (55), respectively.

$$\mu_p^{ref} = \frac{240\,cm^2/V\,s}{MR} \cdot \left(\frac{T}{300\,K}\right)^{-1.09} \tag{67}$$

$$\gamma_n = \frac{1.69}{MX} \tag{68}$$

In Figs 6 and 7 the simulated effective mobilities are compared with those experimental data. It is clear that not only the phonon scattering region for electric fields below 0.5 MV/cm but also the roll-off at higher fields due to surface roughness scattering[30, 40] are described well for the electron mobility. The hole mobilities measured by Takagi *et al.*[30] are smaller than the data published by Watt and Plummer[39] and Walker and Woerlee[40]. In Figs 8 and 9 simulations of *I–V* characteristics with MINIMOS 4

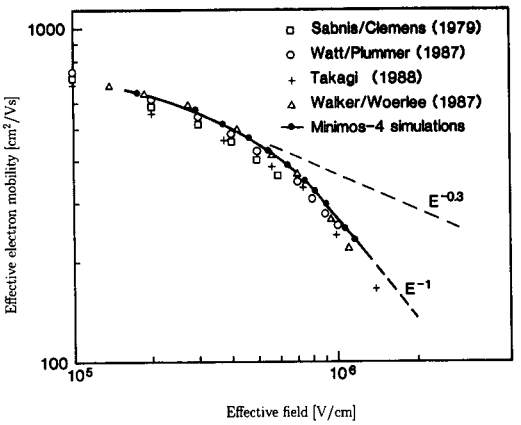

Fig. 6. Effective electron mobility.

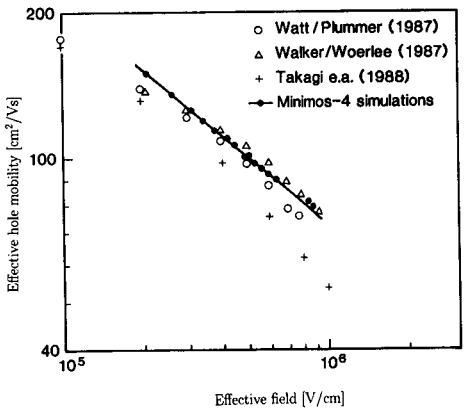

Fig. 7. Effective hole mobility.

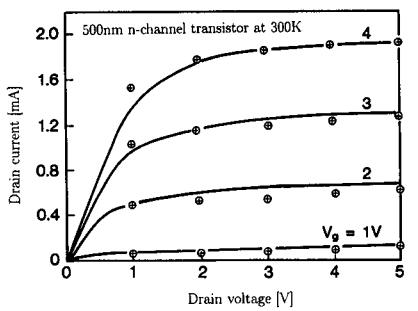

Fig. 8. Comparison of measured (——) and calculated (⊕) I–V characteristic of a MOSFET with 500 nm channel length at 300 K.

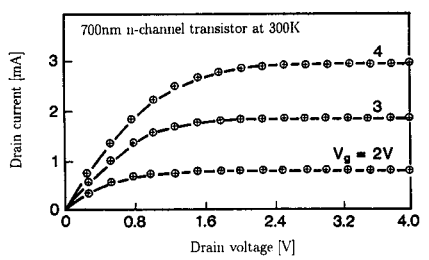

Fig. 9. Comparison of measured (——) and calculated (⊕) I–V characteristic of a MOSFET with 700 nm channel length at 300 K.

are compared to measurements performed at Philips (Thanks to P. J. Biermans, M. J. Bolt and P. H. Woerlee).

The local mobility model in MINIMOS 4 agrees well with the empirical effective mobility versus effective field "universal" mobility curve. Calibrated model parameters are given. Although the physical meaning of the local quantities in the inversion layer itself can be disputed, the calculated effective mobilities and effective electric fields agree with the measurements. Having shown the large validity range of this calibrated local mobility model, and because of the numerical efficiency, it also is recommended for other device simulators.

6.3. The perspective of a Siemens researcher

It is of considerable concern for technology development whether the current/voltage characteristics of a deep submicron MOSFET ($L < 0.3\ \mu$m) can still be reliably predicted with a drift–diffusion type approach for carrier transport modeling. Terminal characteristics are integral quantities and therefore should be relatively insensitive to the exact form of the distributions in the device. It is, however, of interest to find features of the internal distributions that can be detected in the terminal currents. Recently, a series of papers addressing this subject were published from the IBM group[42–44] in which Monte Carlo techniques were used to evaluate the electrical characteristics of deep submicron MOSFETs. An important conclusion drawn from their investigation is the observation of a considerable amount of velocity overshoot that leads to an enhanced transconductance for the ultra short gate length devices. This enhanced transconductance is also reproduced using the extended drift–diffusion approximation provided in MINIMOS 4. We aimed at modeling the MOSFETs considered by the IBM group, using process and device simulation tools. The doping profiles were reconstructed from processing data provided in the literature[45, 46] using a two-dimensional process simulator. In Fig. 10 we show the I–V characteristics of our reconstructed devices as compared to the measured data provided in Ref.[43]. The simulations were performed with a modified version of MINIMOS 4 with the addition of a model for spatial velocity overshoot in the realm of

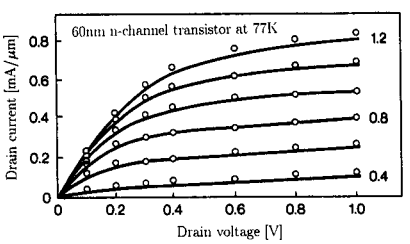

Fig. 10. Comparison of measured (Ref.[32] ——) and calculated (⊕) I–V characteristic of a MOSFET with 60 nm channel length at 77 K.

the extended drift–diffusion model. This can not be modeled within the conventional drift–diffusion approach where $v_{n,p}^{sat}$ is the limiting velocity. We showed[47] that the mobility is primarily a function of the carrier temperature and not of the driving force for the current density. Only if an expansion in this driving force is performed in lowest order is a mobility obtained which only depends on that driving force and accounts for velocity saturation in the usual way[14]. To account for velocity overshoot we have to carry that expansion one step further and collect contributions proportional to the spatial variation of the electronic voltage $UT_{n,p}$. The result of such a calculation is:

$$\mu_{n,p}^{LISFO} = (\mu_{n,p}^{LISF}) \Big/ \left(1 + \eta \cdot \frac{\mu_{n,p}^{LI} \cdot U_{th}}{v_{n,p}^{sat} \cdot UT_{n,p}} \cdot \mathbf{n} \cdot \text{grad}\, UT_{n,p}\right) \quad (69)$$

Here $\mathbf{n}$ is the unit vector in the direction of the current density and $UT_{n,p}$ is the self consistently calculated carrier temperature $UT_{n,p} = k_B \cdot T_{n,p}/q$[16]. η is a dimensionless number of order one and is proportional to the ratio of the high and low field diffusion coefficient. If in a region the particle velocity vector coincides with the direction of a large variation of $UT_{n,p}$ the denominator is reduced and a velocity larger than $v_{n,p}^{sat}$ is possible. In a constant carrier temperature configuration (grad $UT_{n,p} = 0$) there is no velocity overshoot.

To illustrate eqn (69) we consider the drift velocity for a field step located at $x = 0$. On both sides of the field step we assume an electrical field large enough to ensure velocity saturation, for instance $E = 3 \times 10^5$ V/cm for $x < 0$ and $E = 5 \cdot 10^5$ V/cm for $x > 0$. The average carrier energy and drift velocity have to be calculated by utilizing eqn (69). The results for the carrier energy and drift velocity are shown in Figs 11 and 12, respectively. We used for this calculation a saturation velocity 8×10^6 cm/s and an energy relaxation time $\tau_\varepsilon = 0.3$ ps. Carrier temperature and drift velocity were calculated with the hot carrier model of MINIMOS 4. Velocity overshoot occurs near the field step and is approximately 10%. The field step is of course an idealization of a rapid spatial variation. Therefore, we will find an upper estimate for an expected overshoot. In the realistic device situation the overshoot is never larger than 10%.

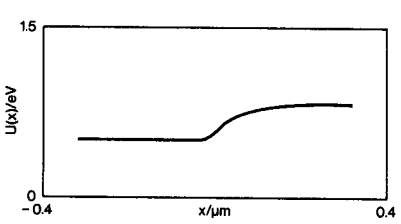

Fig. 11. Carrier temperature for a step like field profile; field step at $x = 0$.

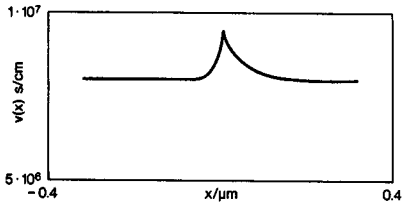

Fig. 12. Carrier drift velocity for a step like field profile; field step at $x = 0$.

In any phenomenological approach to carrier transport modeling the parameters put into the mobility model are of crucial importance. A considerable spread of the parameter values can be found in the literature. The mobility model of MINIMOS was matched to experimental data from several sources for temperatures of 300 K and 77 K as reported in Ref.[20]. This set of parameters also gave the best fit to our typical 4M DRAM MOSFET generation at room temperature. For our investigation the part of the mobility which accounts for velocity saturation is most crucial, whereas the temperature dependence of the low field mobility is not important. A comparison of v_n^{sat} (300 K) and v_n^{sat} (77 K) with the values proposed by the IBM group[43] for long channel devices indicates that our values are too large. However, if we use the values suggested by the IBM group we are not able to obtain a good fit for our 4M DRAM devices. In Fig. 10 we show the calculated MOSFET characteristics using the mobility parameters which have been adjusted to our 4M DRAM technology. No additional fitting is required to obtain the results at 77 K. In the simulation we have included a series resistance of 100 $\Omega\mu$m at both source and drain as reported in Ref.[42].

In Fig. 13 we present the transconductance as a function of gate length and temperature which we obtain in our investigations. The transconductance was calculated with a small signal analysis postprocessor to the MINIMOS program. Figure 11 shows that the enhanced drift–diffusion model indeed

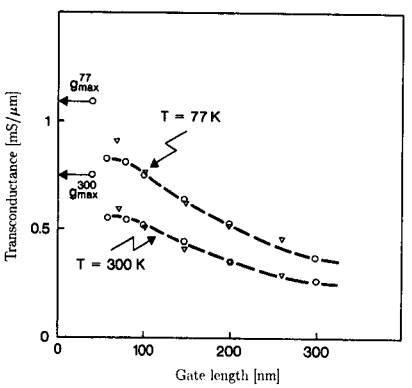

Fig. 13. Comparison of measured (Ref.[32] ▽) and calculated (○) transconductance for different gate lengths at $T = 300$ K and $T = 77$ K. The calculation has been done at $V_{GS} = V_{threshold} + 0.6$ V and $V_{DS} = 0.8$ V; the upper limit $g_{max} = C_{ox} \cdot v_n^{sat}$ for both temperatures is included.

reproduces the measured transconductances very well without any further adjustments. In contrast to the results published in Ref.[43] the effect of the velocity overshoot as modeled in eqn (69) is small, never exceeding 10% variation in transconductance. Although we can reproduce the trend of the measured data very well down to a gate length of 100 nm there is a noticeable deviation of our calculations from the measured data at the extreme end of gate lengths (smaller than 100 nm). At these channel lengths the departure of our results may be due to small deviations in the doping profiles as well as uncertainties in the determination of the gate length which become increasingly important.

Our results demonstrate that extended versions of the drift–diffusion equations can indeed be helpful in evaluating a technology even in the deep submicron region. Provided that the doping profiles can be calculated with sufficient accuracy, the terminal characteristics can still be successfully predicted using mobility parameters which were validated for today's technologies. However, the physical description in the extended drift–diffusion equation might no longer be adequate for the correct determination of the distributions inside the device. Nevertheless the advantage of the phenomenological approach will become obvious in the following: The evaluation of the 42 bias points for the I–V characteristics in Fig. 10 took about 1 h CPU time on a SIEMENS VP200 vector processor using the most sophisticated MOS model that MINIMOS provides (MODEL = HOT). The evaluation of the transconductance (6 bias points for various channel lengths) took another 12 min. The memory requirement for the program including the small signal analysis postprocessor is 14MByte. A further reduction of computational cost is achieved by using a less sophisticated MOS model (MODEL = AVAL), however, at the cost of lower accuracy. These numbers should be compared with the CPU and memory requirements for the Monte Carlo code[43].

We would like to emphasize that although the need for more sophisticated modeling is indisputable there is still room for useful applications of extended drift–diffusion models even in the deep submicron region.

REFERENCES

1. C. Jacoboni, C. Canali, G. Ottaviani and A. A. Quaranta, *Solid-St. Electron.* **20,** 77 (1977).
2. S. Selberherr, *Analysis and Simulation of Semiconductor Devices*. Springer, Wien (1984).
3. S. Selberherr, A. Schütz and H. Pötzl, *IEEE Trans. Electron Devices* **ED-27,** 1540 (1980).
4. H. Brooks, *Phys. Rev.* **83,** 879 (1951).
5. P. P. Debye and E. M. Conwell, *Phys. Rev.* **93,** 693 (1954).
6. C. Canali, G. Majni, R. Minder and G. Ottaviani, *IEEE Trans. Electron Devices* **ED-22,** 1045 (1975).
7. A. Schütz, S. Selberherr and H. Pötzl, *IEEE Trans. Comput. Aided Design* **CAD-1,** 77 (1982).
8. A. Schütz, S. Selberherr and H. Pötzl, *Solid-St. Electron.* **25,** 177 (1982).
9. D. M. Caughey and R. E. Thomas, *Proc. IEEE* **52,** 2192 (1967).
10. K. K. Thornber, *J. appl. Phys.* **51,** 2127 (1980).
11. S. Selberherr, PhD thesis, Technische Universität, Wien (1981).
12. S. Selberherr, A. Schütz and H. Pötzl, *Proc. Process and Device Modeling for Integrated Circuit Design, The Hague*, p. 490. Martinus Nijhoff (1983).
13. W. Müller, L. Risch and A. Schütz, *IEEE Trans. Electron Devices* **ED-29,** 1778 (1982).
14. W. Hänsch and S. Selberherr, *IEEE Trans. Electron Devices* **ED-34,** 1074 (1987).
15. N. D. Arora, J. R. Hauser, and D. J. Roulston, *IEEE Trans. Electron Devices* **ED-29,** 292 (1982).
16. W. Hänsch, Th. Vogelsang, R. Kircher, M. Orlowski, *Solid-St. Electron.* **32,** 839 (1989).
17. N. Ahmad and V. K. Arora, *IEEE Trans. Electron Devices* **ED-33,** 1075 (1986).
18. R. Jaggi, *Helv. phys. Acta* **42,** 941 (1969).
19. R. Jaggi and H. Weibel, *Helv. phys. Acta* **42,** 631 (1969).
20. S. Selberherr, *IEEE Trans. Electron Devices* **ED-36,** 8 (1989).
21. S. S. Li and W. R. Thurber, *Solid-St. Electron.* **20,** 609 (1977).
22. A. K. Henning, N. N. Chan, J. T. Watt and J. D. Plummer, *IEEE Trans. Electron Devices* **ED-34,** 64 (1987).
23. J. M. Dorker and Ph. Leturcq, *Solid-St. Electron.* **24,** 821 (1981).
24. J. W. Slotboom and G. Streutker, *Proc. ESSDERC*, p. 87 (1989).
25. A. G. Sabnis and J. T. Clemens, *Proc. Int. Electron Devices Meeting*, p. 18 (1979).
26. S. C. Sun and J. D. Plummer, *IEEE Trans. Electron Devices* **ED-27,** 1497 (1980).
27. J. Koomen, *Solid-St. Electron.* **16,** 801 (1973).
28. J. R. Brews, *Solid-St. Electron.* **21,** 345 (1978).
29. F. A. VanDeWiele, *Solid-St. Electron.* **22,** 991 (1979).
30. S. Takagi, M. Iwase and A. Toriumi, *Proc. Int. Electron Devices Meeting*, p. 398 (1988).
31. N. D. Arora and G. S. Gildenblat, *IEEE Trans. Electron Devices* **ED-34,** 89 (1987).
32. T. Nishida and C. T. Sah, *IEEE Trans. Electron Devices* **ED-34,** 310 (1987).
33. G. Baccarani and M. R. Wordeman, *IEEE Trans. Electron Devices* **ED-30,** 1295 (1983).
34. D. R. Decker and C. N. Dunn, *J. Electron. Mat.* **4,** 527 (1975).
35. C. Canali and G. Ottaviani, *Phys. Lett.* **32A,** 147 (1970).
36. M. Aoki, K. Yano, T. Masuhara, S. Ikeda and S. Meguro, *Proc. Int. Electron Devices Meeting*, p. 577 (1985).
37. M. Aoki, K. Yano, T. Masuhara, S. Ikeda and S. Meguro, *IEEE Trans. Electron Devices* **ED-34,** 52 (1987).
38. M. Kinugawa, M. Kakumo, T. Usami and J. Matsunaga, *Proc. Int. Electron Devices Meeting*, p. 581 (1985).
39. J. T. Watt and J. D. Plummer, *Proc. VLSI Symposium*, p. 81 (1987).
40. A. J. Walker and P. H. Woerlee, *Proc. ESSDERC*, p. 667 (1987).
41. A. J. Walker and P. H. Woerlee, *Proc. ESSDERC*, p. 265 (1988).
42. S. E. Laux and M. V. Fischetti, *IEEE Electron Device Lett.* **EDL-9,** 467 (1988).
43. G. A. Sai-Halasz, M. R. Wordeman, D. P. Kern, S. Rishton and E. Ganin, *IEEE Electron Devices Lett.* **EDL-9,** 464 (1988).
44. M. V. Fischetti and S. E. Laux, *Phys. Rev.* **B38,** 9721 (1988).

45. G. A. Sai-Halasz, M. R. Wordeman, D. P. Kern, E. Ganin, R. Rishton, D. S. Zicherman, H. Schmid, M. R. Polcari, H. Y. Ng, P. J. Restle, T. H. P. Chang and R. H. Dennard, *IEEE Electron Device Lett.* **EDL-8,** 463 (1987).
46. G. A. Sai-Halasz and H. B. Harrison, *IEEE Electron Device Lett.* **EDL-7,** 534 (1986).
47. W. Hänsch, M. Orlowski and E. Weber, *Proc. ESSDERC* p. 597 (1988).